Compliance Motion Control of the Hydraulic Dual-Arm Manipulator Based on Virtual Decomposition Control

Bolin Sun[1], Min Cheng[1,*], Ruqi Ding[2], Bing Xu[3], Jouni Mattila[4]

1. State Key Laboratory of Mechanical Transmissions, Chongqing University, Chongqing, China, 20220701019@stu.cqu.edu.cn & chengmin@cqu.edu.cn

2. Key Laboratory of Conveyance and Equipment, Ministry of Education, East China Jiaotong University, Nanchang, China, dingruqi0791@sina.com

3. State Key Laboratory of Fluid Power and Mechatronic Systems, Zhejiang University, Hangzhou, China, bxu@zju.edu.cn

4. Faculty of Engineering and Natural Sciences, Tampere University, Tampere, Finland, jouni.mattila@tuni.fi

Abstract.

With the limitation of the single robotic arm's operating capacity, dual-arm collaborative operation has become increasingly prominent. Compared with electrically driven dual-arm manipulator, the closed-chain object transportation task of the hydraulic dual-arm manipulator is more difficult to accurately track the desired motion trajectory, which may cause object deformation or even breakage. To overcome this problem, a compliance motion control method based on virtual decomposition control (VDC) is proposed for the hydraulic dual-arm manipulator in this paper. First of all, for each manipulator of the hydraulic dual-arm system, the VDC method is used to enable its end-effector to accurately track the desired motion trajectory. Then, for the held object, a compliance motion controller is designed to realize the motion control of the object and the internal force control between the object and the manipulator with the aim of minimizing the contact forces between the manipulators and the object. Finally, considering the uncertainty of the object, an adaptive parameter updating method is designed to estimate the inertial parameters and obtain the required net force of the object. Through a simulation study, the advantages of this control method are proved. Compared with the separate position control method of two manipulators, the position and orientation errors of the object are reduced 79.8% and 54.1% by the proposed method, and the internal force and internal moment between the manipulators and the object are also correspondingly reduced 63.9% and 89.4%. In addition, the inertial parameters of the unknown object can be accurately estimated through the adaptive law.

Keywords. Virtual decomposition control, hydraulic dual-arm, compliance motion control, unknown load.

1. INTRODUCTION

With the benefit of high-power density and environmental adaptability [1], hydraulic manipulator has been the main operating mechanism of excavators, cranes and other heavy-duty equipment for undertaking strategic security tasks such as demolition and obstacle removal, material transfer [2, 3]. Due to complexity of working environment and diversity of task demands, the problem of low working efficiency and high safety risk for single hydraulic manipulator is being more and more serious, and the necessity and superiority of heavy-duty dual-arm cooperative manipulation is more and more apparent. However, compared with electrically-driven cooperative dual-arm, the hydraulic dual-arm manipulator has the features of flow/pressure coupling, low damping and oscillation tendency just like the hydraulic single manipulator [4-6], leading to control difficulty of the fine internal force and remarkable error of coordinated motion.

Great progress has been made for the research of electrically-driven dual-arm in recent years, e.g., hybrid force/position control, impedance control [7]. However, none of these methods take into account the uncertainty of hydraulic manipulator system parameters. The existing research results of the electrically-driven dual-arm are difficult to be fully applicable for the hydraulic dual-arm, and still cannot meet its closed-chain operation requirements. The above defects limit the operational efficiency and safety performance of the hydraulic dual-arm. In this paper, a compliance motion control method based on VDC [8] method is proposed for the hydraulic dual-arm manipulator. The aim of the proposed hydraulic dual-arm compliance motion control method is to reduce the position and orientation error when the hydraulic dual-arm manipulator performs the closed-chain collaborative task, and to reduce the internal force and internal moment between the end-effectors of the hydraulic dual-arm manipulator and the held object.

This paper is organized as follows. In Section 2, the VDC approach for the single hydraulic manipulator is briefly introduced. The compliance motion control method of the hydraulic dual-arm manipulator based on VDC method is presented in detail, and the parameter adaptive method for the unknown object is given. In Section 3, the comparison of the simulation results of the proposed method with the individual position control and the results of parameter adaption for the unknown object are given. Finally, the conclusion is given in Section 4.

2. Compliance Motion Control of the Hydraulic Dual-Arm Manipulator

In this section, the hydraulic dual-arm coordination system can be decomposed into the held object and two individual hydraulic manipulators. The control problem of the whole system can be transformed into the control sub-problem of the held object, and the control sub-problem of each manipulator by the concept of virtual stability [8]. Firstly, the VDC method of the individual hydraulic manipulator is briefly introduced. Then, this section is focused on the motion and internal force control of the object held by the hydraulic dual-arm manipulator.

2.1. Virtual Decomposition

The hydraulic manipulator is a nonlinear system with a high degree-of-freedom, which has a complex structure and many parameter uncertainties. Traditional control methods are more difficult to obtain the desired performance. The VDC controller has the features of easy expansion and low computational complexity. The VDC approach is a model-based control method, which can decompose the whole system of hydraulic manipulator with high complexity into subsystems. The controller can be designed at the subsystem level to obtain good control performance, and the stability of the whole system can be ensured through the concept of virtual power flow [8]. For the VDC method, the purpose is to realize the accurate position control of the hydraulic cylinders and then the end-effector of the manipulator. The individual hydraulic manipulator model of the dual-arm manipulator studied in this paper is shown in Figure 1.

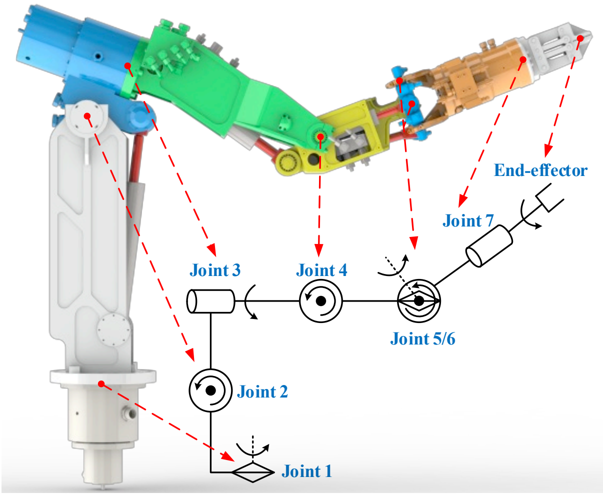

Figure 1. Model of the Single Hydraulic Manipulator

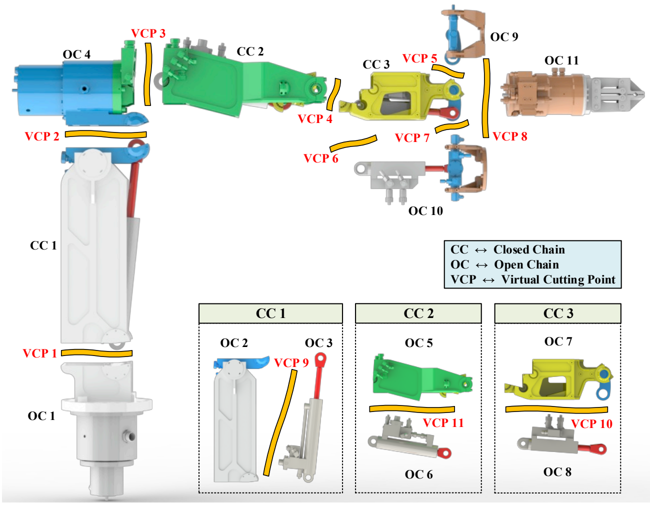

Figure 2. Schematic diagram of Virtual Decomposition for the Hydraulic Manipulator

The schematic diagram of virtual decomposition for the hydraulic manipulator is shown in Figure 2. And the decomposition method is described as follows. First, the hydraulic manipulator is decomposed into open chain, closed chain and object by placing virtual cutting points. Each open chain (OC1, OC4, OC9, OC10 and OC11 in Figure 2) contains one joint and two rigid bodies. The closed chain (CC1, CC2 and CC3 in Figure 2) generally contains two joints (i.e., the prismatic joint of the hydraulic cylinder and its driven revolute joint) and four rigid bodies (two representing the links and the other two representing the hydraulic cylinder). After that, the closed chain can be decomposed into two open chains, i.e., CC1 is decomposed into OC2 and OC3, CC2 is decomposed into OC5 and OC6, and CC3 is decomposed into OC7 and OC8. And the objects are all zero-mass objects, and no motion control specification is assigned to the zero-mass objects.

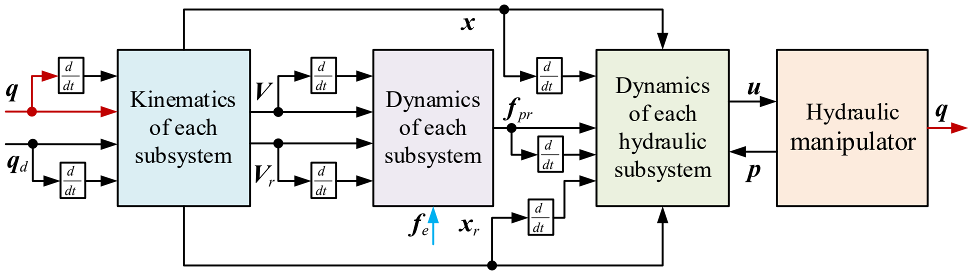

Figure 3. Control Block Diagram for the Single Hydraulic Manipulator

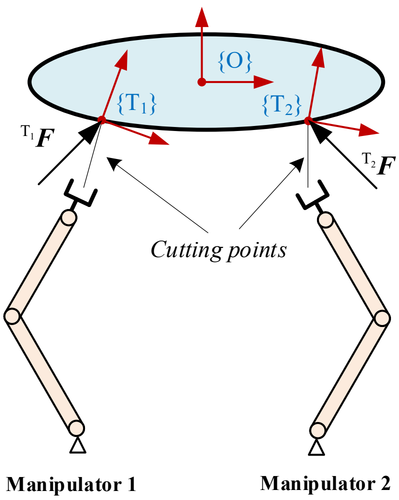

Figure 4. Virtual Decomposition of Dual-Arm Robot

After the hydraulic manipulator is virtually decomposed, each subsystem needs to be modeled mathematically separately to realize the motion control of the hydraulic manipulator [2]. The control block diagram is shown in Figure 3. In Figure 3, $\boldsymbol{q}$ and $\boldsymbol{q}_d$ are the actual joint angle and desired joint angle of the manipulator, respectively, $\boldsymbol{V}$ and $\boldsymbol{V}_r$ are the actual velocity vector and required velocity vector for each subsystem, respectively, $\boldsymbol{f}_e$ is the contact force/moment vector between the end-effector and the environment, $\boldsymbol{p}$ is the pressure vector of the hydraulic system, $\boldsymbol{f}_{pr}$ is the required chamber pressure-induced force, $\boldsymbol{x}$ is the cylinder displacement, $\boldsymbol{x}_r$ is the required cylinder displacement, $\boldsymbol{u}$ is the valve control signal.

In this control method for the individual hydraulic manipulator, the basic idea is to realize control through model feedforward and error feedback. In addition, the adaptive method is used to estimate the uncertain parameters of the hydraulic manipulator in real time online (i.e., the inertia parameters of the manipulator, the friction force of the hydraulic cylinder, the flow coefficient of valves, and the oil volume elastic modulus in the hydraulic system, etc.). So as to realize the high-precision motion control.

To make the VDC applicable, two cutting points are also placed between the end-effectors of the hydraulic dual-arm and the object, as shown in Figure 4. The original system is decomposed into one held object and two separate hydraulic manipulators. In total, there are three frames fixed to the object. The frames $\{T_1\}$ and $\{T_2\}$ are located at the cutting points. The frame {O} which attached to the object is used for motion and internal force control.

2.2. Kinematics and Dynamics of the Held Object

1) Kinematics of the Held Object

When the held object is under free motion, the velocity of the frame {O} can be expressed as

$$ {}^{\mathrm{O}}\boldsymbol{V} = \begin{bmatrix} {}^{\mathrm{O}}\mathbf{R}_{\mathrm{W}}\dot{\boldsymbol{x}} \\ {}^{\mathrm{O}}\mathbf{R}_{\mathrm{W}}\boldsymbol{\omega} \end{bmatrix} = \begin{bmatrix} {}^{\mathrm{O}}\boldsymbol{v} \\ {}^{\mathrm{O}}\boldsymbol{\omega} \end{bmatrix} \tag{1} $$

where $\boldsymbol{x} \in \sim^{3}$ denotes the position vector of the origin of frame {O} expressed in the world frame {W}, $\boldsymbol{\omega} \in \sim^{3}$ denotes the angular velocity vector of the origin of frame {O} expressed in the world frame {W}, ${}^{\mathrm{O}}\mathbf{R}_{\mathrm{W}} \in \sim^{3\times 3}$ denotes the rotation matrix from the object frame {O} to the world frame {W}, ${}^{\mathrm{O}}\boldsymbol{v}$ and ${}^{\mathrm{O}}\boldsymbol{\omega}$ denote the linear and angular vectors of the origin of frame {O} expressed in the frame {O}, respectively.
Since the frame {O}, $\{T_1\}$ and $\{T_2\}$ are all attached to the same object, it follows that

$$ \mathbf{V}_{T} = \begin{bmatrix} {}^{\mathrm{T}_1}\boldsymbol{V} \\ {}^{\mathrm{T}_2}\boldsymbol{V} \end{bmatrix} = {}^{\mathrm{O}}\mathbf{U}_{\mathrm{T}}{}^{T}\mathbf{H}^{T}\,{}^{\mathrm{O}}\boldsymbol{V} \tag{2} $$

with

$$ {}^{\mathrm{O}}\mathbf{U}_{\mathrm{T}} = \mathrm{diag}\left({}^{\mathrm{O}}\mathbf{U}_{\mathrm{T}_1}, {}^{\mathrm{O}}\mathbf{U}_{\mathrm{T}_2}\right) \tag{3} $$

$$ \mathbf{H} = \begin{bmatrix} \mathbf{I}_6 & \mathbf{I}_6 \end{bmatrix} \tag{4} $$

where ${}^{\mathrm{T}_1}\boldsymbol{V}$ and ${}^{\mathrm{T}_2}\boldsymbol{V}$ denote the linear/angular velocity vectors at the cutting points, ${}^{\mathrm{O}}\mathbf{U}_{\mathrm{T}_1} \in \sim^{6\times 6}$ and ${}^{\mathrm{O}}\mathbf{U}_{\mathrm{T}_2} \in \sim^{6\times 6}$ denote the force/moment transformation matrices, and the detailed expression of $\mathbf{U}$ is given in [8], $\mathbf{I}_6 \in \sim^{6\times 6}$ denotes an identity matrix.

2) Dynamics of the Held Object

According to rigid body dynamics, the dynamics of object can be expressed as

$$ \mathbf{M}_{\mathrm{O}}\frac{d}{dt}\left({}^{\mathrm{O}}\boldsymbol{V}\right) + \mathbf{C}_{\mathrm{O}}\left({}^{\mathrm{O}}\boldsymbol{\omega}\right){}^{\mathrm{O}}\boldsymbol{V} + \mathbf{G}_{\mathrm{O}} = {}^{\mathrm{O}}\boldsymbol{F}^{*} \tag{5} $$

where $\mathbf{M}_{\mathrm{O}} \in \sim^{6\times 6}$ is the inertial matrix, $\mathbf{C}_{\mathrm{O}} \in \sim^{6\times 6}$ is the Coriolis and centrifugal matrix, and $\mathbf{G}_{\mathrm{O}} \in \sim^{6}$ is the gravity vector. The detailed expressions of $\mathbf{M}_{\mathrm{O}}$, $\mathbf{C}_{\mathrm{O}}({}^{\mathrm{O}}\boldsymbol{\omega})$ and $\mathbf{G}_{\mathrm{O}}$ are given in [8]. The net force/moment vector ${}^{\mathrm{O}}\boldsymbol{F}^{*} \in \sim^{6}$ can also be expressed as

$$ {}^{\mathrm{O}}\boldsymbol{F}^{*} = {}^{\mathrm{O}}\mathbf{U}_{\mathrm{T}_1}\,{}^{\mathrm{T}_1}\boldsymbol{F} + {}^{\mathrm{O}}\mathbf{U}_{\mathrm{T}_2}\,{}^{\mathrm{T}_2}\boldsymbol{F} \tag{6} $$

where ${}^{\mathrm{T_1}}\boldsymbol{F} \in \sim^{6}$ and ${}^{\mathrm{T_2}}\boldsymbol{F} \in \sim^{6}$ denote the force/moment vectors in frame {T1} and {T2} at the cutting points. By introducing an internal force vector, the force/moment vectors at the cutting points can be resolved from (6) as

$$\mathbf{F}_T = \begin{bmatrix} {}^{\mathrm{T_1}}\boldsymbol{F} \\ {}^{\mathrm{T_2}}\boldsymbol{F} \end{bmatrix} = {}^{\mathrm{T}}\mathbf{U}_{\mathrm{O}} \begin{bmatrix} \boldsymbol{\Omega}_m & \boldsymbol{\Omega}_f \end{bmatrix} \begin{bmatrix} {}^{\mathrm{O}}\boldsymbol{F}^{*} \\ \boldsymbol{\eta} \end{bmatrix} \tag{7}$$

where ${}^{\mathrm{T}}\mathbf{U}_{\mathrm{O}} = {}^{\mathrm{O}}\mathbf{U}_{\mathrm{T}}^{-1}$ is defined by (3). A possible way to define the internal forces is to let the internal forces characterize the squeeze force/moment vectors among the end-effectors. As in [9], the matrix $\boldsymbol{\Omega}_m \in \sim^{12\times 6}$ and the matrix $\boldsymbol{\Omega}_f \in \sim^{12\times 6}$ are governed by

$$\boldsymbol{\Omega}_m = \frac{1}{2}\begin{bmatrix} \mathbf{I}_6 & \mathbf{I}_6 \end{bmatrix}^T \tag{8}$$

$$\boldsymbol{\Omega}_f = \begin{bmatrix} \mathbf{I}_6 & -\mathbf{I}_6 \end{bmatrix}^T \tag{9}$$

Then, the internal force vector can be defined as

$$\boldsymbol{\eta} = \boldsymbol{\eta}_{1,2} \tag{10}$$

where $\boldsymbol{\eta}_{1,2} \in \sim^{6}$ denotes the internal force/moment vector exerted from the 1st end-effector to the 2nd end-effector, expressed in frame {O}. Because the matrix $\begin{bmatrix} \boldsymbol{\Omega}_m & \boldsymbol{\Omega}_f \end{bmatrix} \in \sim^{12\times 12}$ is of full rank, there must exist a matrix $\boldsymbol{\Phi} \in \sim^{6\times 12}$ such that

$$\boldsymbol{\Phi} = \frac{1}{2}\begin{bmatrix} \mathbf{I}_6 & -\mathbf{I}_6 \end{bmatrix} \tag{11}$$

Thus, the internal force/moment vector can be obtained from (7) by using the force/moment measurements at the end-effectors as

$$\boldsymbol{\eta} = \boldsymbol{\Phi}\, {}^{\mathrm{O}}\mathbf{U}_{\mathrm{T}} \mathbf{F}_T \tag{12}$$

2.3. Motion and Internal Force Control of the Held Object

1) Motion and Internal Force Control Specifications

Define a frame {D}, whose origin and orientation represent the desired position and orientation of the frame {O}. The motion control objective is to make frame {O} track frame {D}. Meanwhile, let $\boldsymbol{\eta}_d \in \sim^{6}$ be the desired internal force coordinate vector. The internal force control objective is

$$\boldsymbol{\eta}_d - \boldsymbol{\eta} \to \mathbf{0} \tag{13}$$

2) Required Velocity and Force/Moment Vectors

The required velocity vector of frame {O} is designed as

$${}^{\mathrm{O}}\boldsymbol{V}_r = {}^{\mathrm{O}}\boldsymbol{V}_d + \mathbf{E} \tag{14}$$

$${}^{\mathrm{O}}\boldsymbol{V}_d = \begin{bmatrix} {}^{\mathrm{O}}\mathbf{R}_{\mathrm{W}}\dot{\boldsymbol{x}}_d \\ {}^{\mathrm{O}}\mathbf{R}_{\mathrm{W}}\boldsymbol{\omega}_d \end{bmatrix} \tag{15}$$

$$\mathbf{E} = \begin{bmatrix} k_x \, {}^{\mathrm{O}}\mathbf{R}_{\mathrm{W}} \left(\boldsymbol{x}_d - \boldsymbol{x} \right) \\ k_\omega \, {}^{\mathrm{O}}\boldsymbol{\mu} \end{bmatrix} \tag{16}$$

where $k_x > 0$ and $k_\omega > 0$ are two constants, $\boldsymbol{x}_d \in \sim^{3}$ denotes the desired position (the origin of frame $\{\mathrm{D}\}$) vector, $\boldsymbol{\omega}_d \in \sim^{3}$ denotes the desired angular velocity vector, and ${}^{\mathrm{O}}\boldsymbol{\mu} \in SO^3$ denotes the vector part of a quaternion representing the rotation from frame $\{\mathrm{O}\}$ to frame $\{\mathrm{D}\}$.

According to (2), the required linear/angular velocity vectors of the end-effectors can be designed as

$$\mathbf{V}_{Tr} = \begin{bmatrix} {}^{\mathrm{T_1}}\boldsymbol{V}_r \\ {}^{\mathrm{T_2}}\boldsymbol{V}_r \end{bmatrix} = {}^{\mathrm{O}}\mathbf{U}_{\mathrm{T}}{}^{T} \left[\mathbf{H}^{T} \, {}^{\mathrm{O}}\boldsymbol{V}_r + \boldsymbol{\Phi}^{T} \mathbf{A}_{f\eta} \left(\tilde{\boldsymbol{\eta}}_d - \tilde{\boldsymbol{\eta}} \right) \right] \tag{17}$$

where $\mathbf{A}_{f\eta} \in \sim^{6\times6}$ is a diagonal positive-definite matrix, $\tilde{\boldsymbol{\eta}}_d$ and $\tilde{\boldsymbol{\eta}}$ can be obtained by

$$\dot{\tilde{\boldsymbol{\eta}}}_d = \mathbf{C}_{f\eta} \left(\boldsymbol{\eta}_d - \tilde{\boldsymbol{\eta}}_d \right) \tag{18}$$

$$\dot{\tilde{\boldsymbol{\eta}}} = \mathbf{C}_{f\eta} \left(\boldsymbol{\eta} - \tilde{\boldsymbol{\eta}} \right) \tag{19}$$

where $\mathbf{C}_{f\eta} \in \sim^{6\times6}$ is a diagonal positive-definite matrix.

Note that the second term on the right hand side of (17) contains the filtered internal force error vector that is added to the complementary motion configuration space spanned by $\boldsymbol{\Phi}^{T}$. This term is used to achieve the filtered internal force control characterized by $\tilde{\boldsymbol{\eta}}_d - \tilde{\boldsymbol{\eta}} \to \mathbf{0}$. Equations (18) and (19) define two low-pass filters to be used to filter out the desired and actual internal forces, respectively. The cut-off frequency of the two filters is determined by matrix $\mathbf{C}_{f\eta}$.

Based on the unknown inertial parameters of the held object in the real situation, an adaptive parameter updating approach is used to estimate the dynamics of the unknown object in this paper. The linear parametrization expression of (5) can be written as

$$\mathbf{M}_{\mathrm{O}} \frac{d}{dt}\left({}^{\mathrm{O}}\boldsymbol{V}_r \right) + \mathbf{C}_{\mathrm{O}} \left({}^{\mathrm{O}}\boldsymbol{\omega} \right) {}^{\mathrm{O}}\boldsymbol{V}_r + \mathbf{G}_{\mathrm{O}} = \mathbf{Y}_{\mathrm{O}} \boldsymbol{\theta}_{\mathrm{O}} \tag{20}$$

where $\mathbf{Y}_{\mathrm{O}} \in \sim^{6\times13}$ is a regression matrix, $\boldsymbol{\theta}_{\mathrm{O}} \in \sim^{13}$ is a parameter vector. For the unknown object, $\boldsymbol{\theta}_{\mathrm{O}}$ is generally uncertain [10, 11].

So, the required net force/moment vector of the held object is written as

$${}^{\mathrm{O}}\boldsymbol{F}_r^{*} = \mathbf{Y}_{\mathrm{O}} \hat{\boldsymbol{\theta}}_{\mathrm{O}} + \mathbf{K}_{\mathrm{O}} \left({}^{\mathrm{O}}\boldsymbol{V}_r - {}^{\mathrm{O}}\boldsymbol{V} \right) \tag{21}$$

where $\mathbf{K}_{\mathrm{O}} \in \sim^{6\times6}$ is a positive-definite gain matrix, $\hat{\boldsymbol{\theta}}_{\mathrm{O}} \in \sim^{13}$ denotes the estimate of $\boldsymbol{\theta}_{\mathrm{O}} \in \sim^{13}$.The specific parameter adaptive function and adaptive process can be referred to [8].

After ${}^{\mathrm{O}}\boldsymbol{F}_r^{*} \in \sim^{6}$ is obtained from (21) and $\boldsymbol{\eta}_d \in \sim^{6}$ is obtained from the internal force control specification which mentioned below, the required force/moment vectors at the end-effectors are designed from (7) as

$$\mathbf{F}_{Tr} = \begin{bmatrix} {}^{\mathrm{T}_1}\boldsymbol{F}_r \\ {}^{\mathrm{T}_2}\boldsymbol{F}_r \end{bmatrix} = {}^{\mathrm{T}}\mathbf{U}_{\mathrm{O}} \left[\boldsymbol{\Omega}_m \quad \boldsymbol{\Omega}_f \right] \begin{bmatrix} {}^{\mathrm{O}}\boldsymbol{F}_r^* \\ \boldsymbol{\eta}_d \end{bmatrix} \tag{22}$$

3) Internal Force Optimization

The desired internal force vector $\boldsymbol{\eta}_d \in \sim^6$ can be designed in different ways. Most commonly, it can be used to minimize the contact forces/moments at the end-effectors, that is, find $\boldsymbol{\eta}_d$ to minimize $\mathbf{F}_T{}^T \mathbf{W}_\eta \mathbf{F}_T$ under (13), where $\mathbf{W}_\eta$ is a weighting matrix and $\mathbf{F}_T$ is being defined by (7). For this purpose, equation (7) can be re-written as

$$\mathbf{F}_T = \mathbf{A}_\eta \boldsymbol{\eta} + \mathbf{B}_\eta \tag{23}$$

with

$$\mathbf{A}_\eta = {}^{\mathrm{T}}\mathbf{U}_{\mathrm{O}} \boldsymbol{\Omega}_f \tag{24}$$

$$\mathbf{B}_\eta = {}^{\mathrm{T}}\mathbf{U}_{\mathrm{O}} \boldsymbol{\Omega}_m \, {}^{\mathrm{O}}\boldsymbol{F}^* \tag{25}$$

In the sense of minimizing $\mathbf{F}_T{}^T \mathbf{W}_\eta \mathbf{F}_T$, the least-square solution for $\boldsymbol{\eta}$ is

$$\boldsymbol{\eta} = -\left(\mathbf{A}_\eta{}^T \mathbf{W}_\eta \mathbf{A}_\eta \right)^{-1} \mathbf{A}_\eta{}^T \mathbf{W}_\eta \mathbf{B}_\eta \tag{26}$$

In line with (26), the desired internal force coordinate vector $\boldsymbol{\eta}_d$ is designed as

$$\boldsymbol{\eta}_d = -\left(\mathbf{A}_\eta{}^T \mathbf{W}_\eta \mathbf{A}_\eta \right)^{-1} \mathbf{A}_\eta{}^T \mathbf{W}_\eta \mathbf{B}_{\eta r} \tag{27}$$

$$\mathbf{B}_{\eta r} = {}^{\mathrm{T}}\mathbf{U}_{\mathrm{O}} \boldsymbol{\Omega}_m \, {}^{\mathrm{O}}\boldsymbol{F}_r^* \tag{28}$$

4) Dual-arm motion/force control frame

The block diagram of the hydraulic dual-arm compliance motion control based on VDC is shown in Figure 5. For the held object, the desired velocity of the object is given, the object required velocity is obtained from the compliance motion controller. The actual velocity of the object is obtained according to the coordination constraint relationship between the dual-arm and the object and fed back to the compliance motion controller [12]. In addition, the required velocity of the dual-arm end-effectors can be obtained from the coordination constraint relationship based on the required velocity of the object. Then, the desired joint angle and angular velocity of the dual-arm are obtained by inverse kinematics, and the actual joint angle and angular velocity of the dual-arm are obtained by the dual-arm environment. The inverse kinematics solution method for the hydraulic manipulator which studied in this paper can be obtained from [13].

And then, the two hydraulic manipulators are controlled separately by VDC method, and the valve control voltage signal of each hydraulic cylinder of the manipulators are input to the dual-arm environment. The actual joint angles of the dual-arm are output from the dual-arm environment to the forward kinematics of the manipulators to obtain the end-effectors motion trajectory, and the output contact force is fed back to the compliance motion controller for the object. And, the forward kinematics can also be obtained from [13]. Finally, the whole closed-loop control is formed to realize the compliance motion control of the hydraulic dual-arm cooperative manipulation.

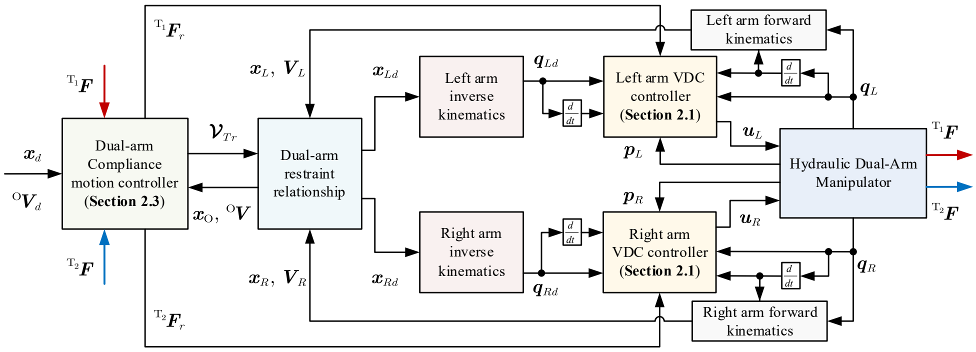

Figure 5. Block Diagram of the Dual-Arm Compliance Motion Control

3. SIMULATION STUDY

3.1. *Simulation Model and Settings*

In this section, the feasibility of the proposed control method is verified for hydraulic dual-arm to complete the task of closed chain collaboration. To verify the advantage of the proposed method, the end-effector position control (PC) method is used for comparison with it, i.e., the desired trajectory of the end-effector of each hydraulic manipulator is obtained by constraint relation according to the desired motion trajectory of the object, and then each arm is controlled by VDC method to track this trajectory.

The MATLAB/Simulink is used to build the simulation platform for hydraulic dual-arm manipulator and carry out a real-time simulation, which is composed of two hydraulic manipulators from Section II. The simulation model and frame configuration are shown in Figure 6, and all the system parameters settings of the simulation model are based on the experimental prototype from the [13]. In the simulation, the desired motion trajectory of the frame {O} on the object which set in the Cartesian coordinates is a circular trajectory with a center of [1.5m, 1.3m] (located in the yOz plane) and a radius of 0.25m, which can be expressed as

$$x = 0 \quad y = 1.5 \quad z = 1.05 \quad if \;\; t < 2$$

$$\boldsymbol{x}_d \Rightarrow \begin{cases} x = 0 \\ y = 0.25\sin\big(2\pi(t-2)/T\big) + 1.5 \quad if \;\; 2 \le t < 12 \\ z = -0.25\cos\big(2\pi(t-2)/T\big) + 1.3 \end{cases} \tag{29}$$

where t is the simulation time , $T = 10$ s is the motion period.

The total simulation time is set to 12 s, using a fixed step solver, and the simulation step is set to 0.001 s. The simulation is divided into two stages. In the first stage (0~2 s), as shown in the yellow area in Figure 7-9 below, the object is held still by dual-arm manipulator. And in the second stage (2~12 s), as shown in the green area in Figure 7-9 below, the object is held by dual-arm manipulator to do the above circular motion. And the main parameters used in the simulation model are listed in Table I.

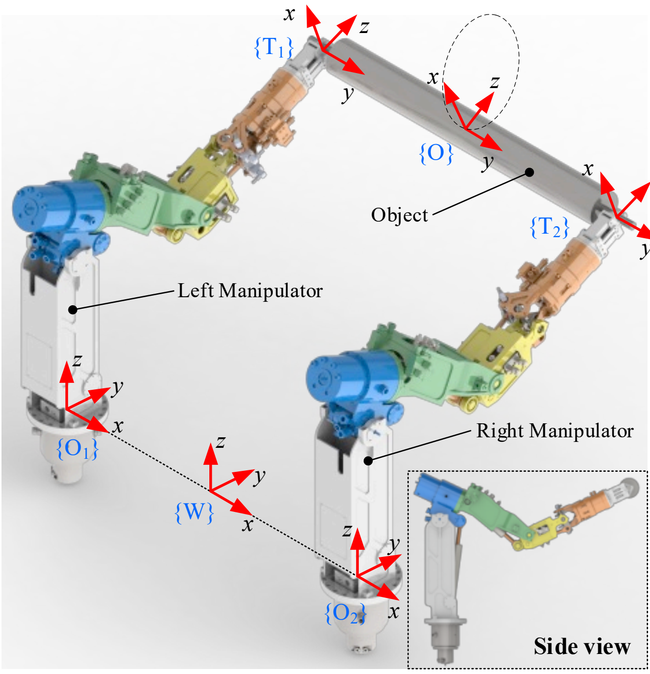

Figure 6. Simulation model of the Hydraulic Dual-Arm Manipulator

Table I. Main parameters used in the simulation model

Parameter	Symbol	Value
Gain of position error	k_x	0.6
Gain of orientation error	k_ω	0.6
Gain matrix of filtered internal force error vector	$\mathbf{A}_{f\eta}$	$10^{-5}\cdot\mathbf{I}_6$
Cut-off frequency matrix of the filter	$\mathbf{C}_{f\eta}$	$30\cdot\mathbf{I}_6$
Gain matrix of velocity error vector	$\mathbf{K}_O$	$100\cdot\mathbf{I}_6$
Weighting matrix for internal force optimization	$\mathbf{W}_\eta$	$\mathbf{I}_{12}$

3.2. Simulation results

Note that the solid lines in Figures 7 and 8 represent the position error, orientation error, internal force and internal moment of the object in the three directions of xyz under the PC method, respectively, while the dotted lines in Figures 7 and 8 represent the CMC method.

A comparison of the object position and orientation errors for separate position control (PC) and compliance motion control (CMC) is shown in Figure 7. During the period when the object is held still (0~2 s) by the arms, the position and orientation errors of the object do not change much, but the CMC method is significantly better than the PC method. The position and orientation errors of the object using the CMC method are basically zero. In the subsequent process, the position and orientation errors of the object for circular motion (2~12 s) is also similar. It always has a large error in the z direction by the PC method, mainly because the inertial parameters of the unknown object cannot be accurately estimated.

Compared with the PC method, the position and orientation errors of the object are reduced 79.8% and 54.1% by the proposed method (CMC method). As a whole, the accuracy of coordinated motion of dual-arm is improved.

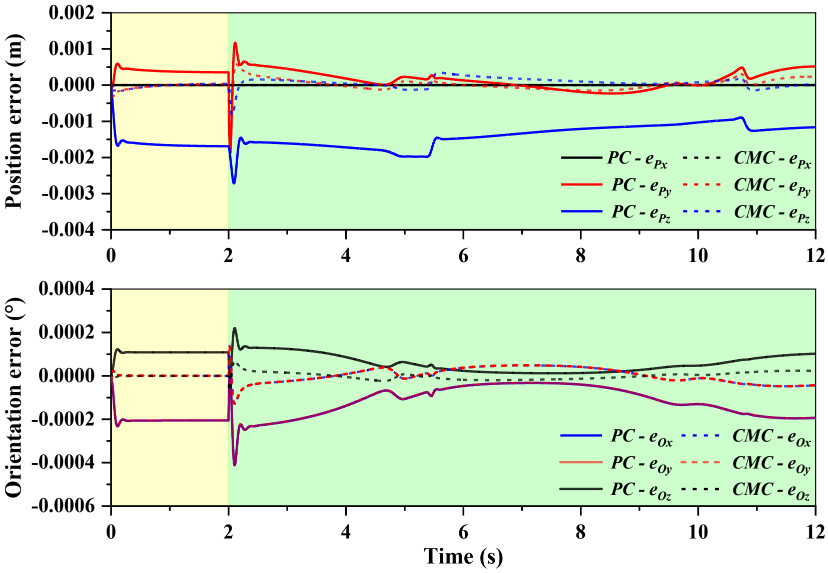

Figure 7. Position and orientation errors

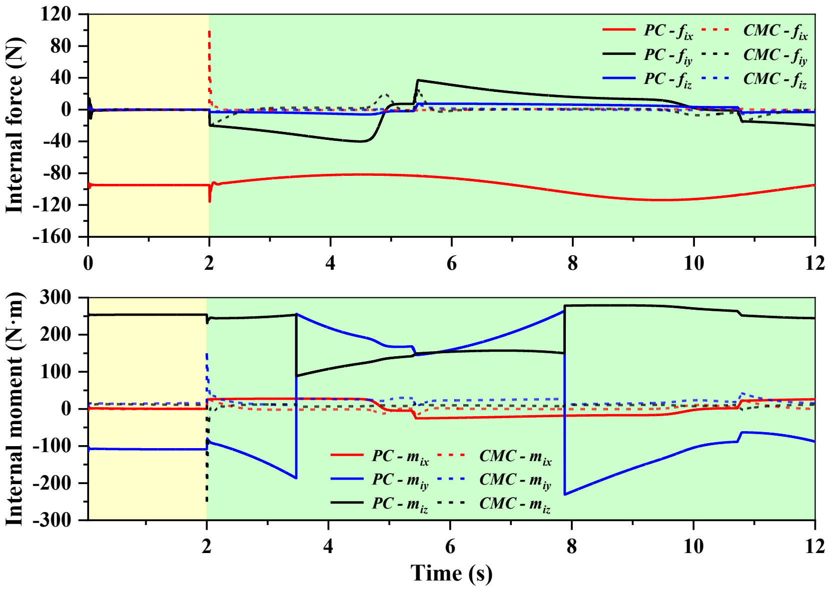

Figure 8. Internal force and moment

Then, a comparison of the internal force/moment results is shown in Figure 8. From the perspective of the overall control effect, compared with the PC method, the control effects of the internal force and the internal moment of the CMC method are maintained at a small value. Compared with the PC method, the internal force and moment between the arms and the object are also correspondingly reduced 63.9% and 89.4% by the CMC method.

The control effects of different control methods are shown in Table II. Note that the error reduction ratio here refers to the reduction of their maximum values in the three directions of xyz, and the reduction ratio of internal force and internal moment here also refers to the reduction of their maximum values in the three directions of xyz.

Since the inertia parameters of the held object are difficult to obtain in advance in real situations, the parameter adaptation method is used to estimate inertial parameters of the unknown object in the simulation experiment. Among all inertial parameters, the mass has a great influence on the accuracy of the motion. Therefore, only the results of object mass adaptation are presented here, as shown in Figure 9.

As shown in the dashed line, the real mass of the object model in the simulation is 402.726 kg, and the adaptive value of the object mass rises rapidly after the motion starts and gradually stabilizes around the real value. It can also be seen that the error between the adaptive value and the real value is small which below ±1.5%.

Table II. Comparison of the different control methods

Parameter	PC	CMC
Position error (m)	2.71×10^{-3}	0.547×10^{-4}
Orientation error (°)	4.11×10^{-4}	1.89×10^{-4}
Internal force (N)	115.81	41.81
Internal moment (N·m)	279.28	29.60

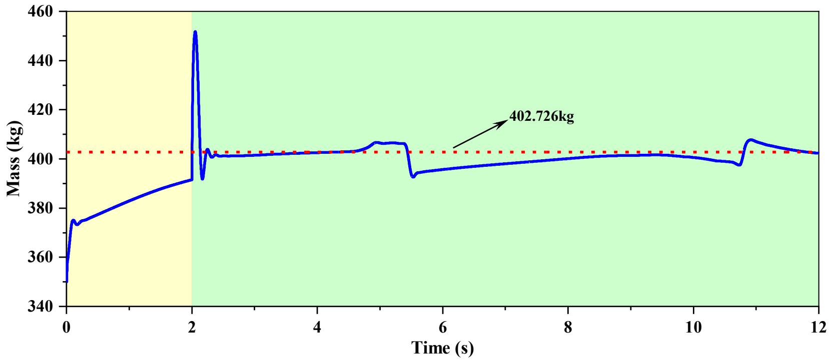

Figure 9. Adaptive Results of Object Mass

4. CONCLUSION

In this paper, we propose a compliance motion control method of hydraulic dual-arm based on virtual decomposition control for the closed-chain collaborative task, and verify the effectiveness of the method by simulation. The simulation results show that the compliance motion control method of hydraulic dual-arm can effectively reduce the position and orientation errors by 79.8% and 54.1% of the end-effectors of the dual-arm, and also reduce the internal force/moment by 63.9% and 89.4% between the end-effectors and the object. In addition, the method can make a more accurate estimation of the inertia parameters of the unknown object such as mass, and the error can be as low as ±1.5%.

In the future, the research will focus on the study of the hydraulic dual-arm system under the constrained motion.

5. ACKNOWLEDGMENT

This work is supported by the National Natural Science Foundation of China under Grant 52075055 and 52111530069, the Natural Science Foundation of Chongqing, China under Grant cstc2020jcyjmsxmX0780m.

6. REFERENCES

[1] R. Ding, M. Cheng, L. Jiang, and G. Hu, "Active Fault-Tolerant Control for Electro-Hydraulic Systems With an Independent Metering Valve Against Valve Faults," *IEEE Trans. Ind. Electron.*, vol. 68, no. 8, pp. 7221-7232, 2021.

[2] J. Koivumäki and J. Mattila, "High performance nonlinear motion/force controller design for redundant hydraulic construction crane automation," *Autom. Constr.*, vol. 51, pp. 59-77, 2015.

[3] X. Rong, Y. Li, J. Ruan, and B. Li, "Design and simulation for a hydraulic actuated quadruped robot," *J. Mech. Sci. Technol.*, vol. 26, no. 4, pp. 1171-1177, 2012.

[4] J. Koivumaki and J. Mattila, "Stability-Guaranteed Force-Sensorless Contact Force/Motion Control of Heavy-Duty Hydraulic Manipulators," *IEEE Trans. Rob.*, vol. 31, no. 4, pp. 918-935, 2015.

[5] M. Cheng, J. Zhang, B. Xu, R. Ding, and J. Wei, "Decoupling Compensation for Damping Improvement of the Electrohydraulic Control System With Multiple Actuators," *IEEE/ASME Trans. Mechatron.*, vol. 23, no. 3, pp. 1383-1392, 2018.

[6] S. H. Hyon, D. Suewaka, Y. Torii, N. Oku, and H. Ishida, "Development of a fast torque-controlled hydraulic humanoid robot that can balance compliantly," in *2015 IEEE-RAS 15th International Conference on Humanoid Robots (Humanoids)*, 2015, pp. 576-581.

[7] C. Smith *et al.*, "Dual arm manipulation—A survey," *Rob. Auton. Syst.*, vol. 60, no. 10, pp. 1340-1353, 2012.

[8] W. H. Zhu, *Virtual decomposition control: Toward hyper degrees of freedom robots*, 1st ed. (Springer Tracts in Advanced Robotics). Berlin: Springer Berlin, Heidelberg, 2010.

[9] W. H. Zhu, "On adaptive synchronization control of coordinated multirobots with flexible/rigid constraints," *IEEE Trans. Rob.*, vol. 21, no. 3, pp. 520-525, 2005.

[10] Z. Wen-Hong and J. D. Schutter, "Adaptive control of mixed rigid/flexible joint robot manipulators based on virtual decomposition," *IEEE Transactions on Robotics and Automation*, vol. 15, no. 2, pp. 310-317, 1999.

[11] W.-H. Zhu and J.-C. Piedboeuf, "Adaptive Output Force Tracking Control of Hydraulic Cylinders With Applications to Robot Manipulators," *J. Dyn. Syst. Meas. Contr.*, vol. 127, no. 2, pp. 206-217, 2004.

[12] J. J. Duan, Y. H. Gan, M. Chen, and X. Z. Dai, "Symmetrical adaptive variable admittance control for position/force tracking of dual-arm cooperative manipulators with unknown trajectory deviations," *Rob. Comput. Integr. Manuf.*, vol. 57, pp. 357-369, 2019.

[13] M. Cheng, Z. N. Han, R. Q. Ding, J. H. Zhang, and B. Xu, "Development of a redundant anthropomorphic hydraulically actuated manipulator with a roll-pitch-yaw spherical wrist," *Frontiers of Mechanical Engineering*, vol. 16, no. 4, pp. 698-710, Dec 2021.

Biographies

Bolin Sun received the B.S. degree in mechanical engineering from Shandong University of Science and Technology, Qingdao, China, in 2020. Since 2022, he has been working toward the Ph.D. degree in mechanical engineering with the State Key Laboratory of Mechanical Transmission, Chongqing University, Chongqing, China. His research interests include electrohydraulic control systems of mobile machinery and motion control of hydraulic systems.

Min Cheng received the B.S. and Ph.D. degrees in mechatronics from Zhejiang University, Hangzhou, China, in 2009 and 2015, respectively. He is currently a Professor with the State Key Laboratory of Mechanical Transmissions, Chongqing University, Chongqing, China. His research interests include electrohydraulic control systems of mobile machinery, energy saving and motion control of hydraulic systems, and mechatronic systems design.

Ruqi Ding received the B.S. degree in mechatronics engineering from Nanchang University, Nanchang, China in 2009, and the Ph.D. degree in fluid power transmission and control from Zhejiang University, Hangzhou, China, in 2015. He is currently a Professor with the Key Laboratory of Conveyance and Equipment, Ministry of Education, East China Jiaotong University. His research interests include electrohydraulic control systems, as well as the motion control of hydraulic manipulators.

Bing Xu received the Ph.D. degree in fluid power transmission and control from Zhejiang University, Hangzhou, China, in 2001. He is currently a Professor and a Doctoral Tutor in the Institute of Mechatronic Control Engineering, and the Deputy Director of the State Key Laboratory of Fluid Power Transmission and Control, Zhejiang University. He has authored or co-authored more than 200 journal and conference papers and authorized 49 patents. Professor Xu is a Chair Professor of the Yangtze River Scholars Programme, and a science and technology innovation leader of the Ten Thousand Talent Programme.

Jouni Mattila received the M.S. and Ph.D. degrees in automation engineering from the Tampere University of Technology, Tampere, Finland, in 1995 and 2000, respectively. He is currently a Professor with the Unit of Automation Technology and Mechanical Engineering, Tampere University, Tampere, Finland. His research interests include machine automation, nonlinear model-based control of hydraulic robotic manipulators, and energy-efficiency of fluid power systems.